

pubs.acs.org/cm Article

Transient Competitors to Modulate Dynamic Covalent Cross-Linking of Recombinant Hydrogels

Aidan E. Gilchrist, Yueming Liu, Katarina Klett, Yu-Chung Liu, Sofía Ceva, and Sarah C. Heilshorn*



Cite This: Chem. Mater. 2023, 35, 8969-8983



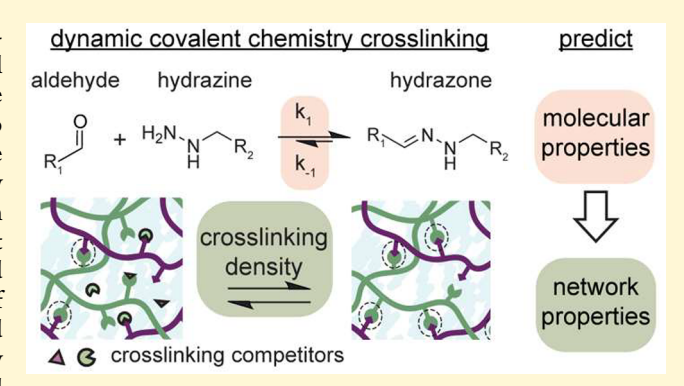
ACCESS I

III Metrics & More

Article Recommendations

s Supporting Information

ABSTRACT: Hydrogels cross-linked by dynamic covalent chemistry (DCC) are stiff and remodelable, making them ideal biomimetics for tissue engineering applications. Due to the reversibility of DCC cross-links, the opportunity exists to transiently control hydrogel network formation through the use of small molecule competitors. Specifically, we incorporate low molecular weight competitors that reversibly disrupt the formation of hydrazone cross-links as they diffuse through a recombinant hydrogel. Using complementary experimental, computational, and theoretical polymer physics approaches, we present a family of competitors that predictably alter hydrogel gelation time and mechanics. By changing the competitor chemistry, we connect key reaction parameters (forward and reverse reactions rates and



thermodynamic equilibrium constants) to the delayed onset of a percolated network, increased hydrogel gelation time, and transient control of hydrogel stiffness. Using human intestinal organoids as a model system, we demonstrate the ability to tune gelation kinetics of a recombinant hydrogel for uniform encapsulation of individual, patient-derived stem cells and their proliferation into three-dimensional structures. Taken together, our data establish a validated framework to relate molecular-level parameters of transient competitors to predicted macromolecular-network properties. As interest in biomimetic, DCC-cross-linked hydrogels continues to grow, these results will enable the rationale design of bespoke, dynamic biomaterials for tissue engineering.

■ INTRODUCTION

Hydrated, polymeric scaffolds, termed hydrogels, are widely used for tissue engineering and regenerative medicine approaches. Hydrogels are especially advantageous for threedimensional cell culture as they are largely composed of water and are readily tuned to mimic essential features of the native tissue microenvironment.² Biomechanical and biochemical cues, such as stiffness and cell-adhesive ligand density, can be intentionally designed into the hydrogel by controlling initial synthesis parameters.³⁻⁶ Another important property that can be incorporated into hydrogel design is the ability of the material to be remodeled by encapsulated cells, which reflects the way that cells remodel the native microenvironment.^{7–10} Cell-mediated hydrogel remodeling is implicated in driving cell phenotype, including cell migration and stem cell differentiation. In chemical hydrogels with static crosslinks, remodelability is often achieved by incorporating hydrolytically cleavable components into the material; however, this process is irreversible. In contrast, physical hydrogels with dynamic cross-links formed through physical interactions between polymer chains are inherently remodelable, but the resulting materials are typically quite weak (<0.1 kPa). As an alternative approach, dynamic covalent chemistry (DCC) has emerged as a cross-linking strategy that enables synthesis of stiff (>1 kPa)^{22,23}

remodelable hydrogels for tissue engineering applications. While covalent bonds are generally thought of as static, DCC bonds are strong and reversible, making them an ideal choice for synthesis of remodelable hydrogels. 24–26

Hydrazone chemistry is a particularly useful class of DCC for tissue engineering approaches. 27,28 Compared to other DCC strategies, the forward and reverse reactions rates of hydrazone chemistry are appreciable at physiological conditions ($\sim 10^{-1}-10^1~\text{s}^{-1}$). 29,30 Additionally, the cross-linking reaction is spontaneous, 31 requiring no ultraviolet light or radical initiation, which eliminates confounding reactive radicals that can occur in other cross-linking strategies. Despite these advantages, hydrazone-cross-linked hydrogels have some limitations. Namely, the reaction proceeds rapidly, which quickly produces a percolated network of polymers that form a gel. This rapid gelation rate can result in inhomogeneous mixing of the polymer precursors and

Received: June 22, 2023 Revised: September 27, 2023 Accepted: October 10, 2023 Published: October 27, 2023





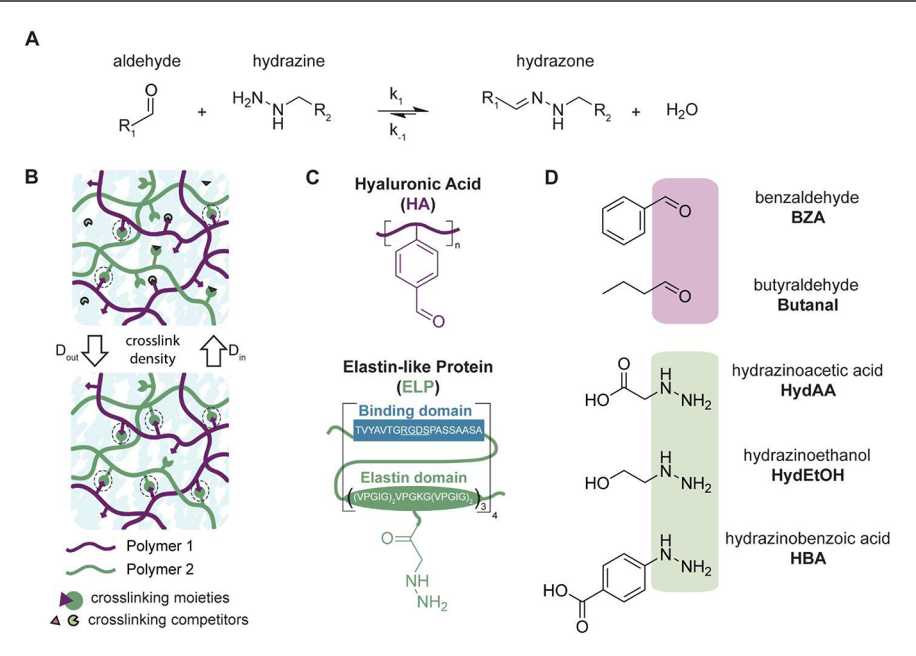


Figure 1. Library of competitors for transient disruption of hydrazone cross-links. A. The reaction of aldehyde and hydrazine to form hydrazone and water is a dynamic, reversible reaction that occurs under physiological conditions. B. Schematic of a transient competitor for modulating cross-linking density. Small molecule competitors can diffuse into the hydrogel to temporarily decrease cross-linking density or diffuse out of the hydrogel to allow cross-links to form. Cross-linking sites are circled with dotted lines. C. Schematic of HELP matrix. HELP is composed of benzaldehyde-modified hyaluronic acid (HA-BZA) and hydrazine-modified elastin-like protein (ELP-HYD). When mixed, these two components form an HA-ELP (HELP) hydrogel. D. The library of competitors include small molecules with either aldehyde or hydrazine functional groups that can react with ELP-HYD or HA-BZA, respectively. Each group contains a competitor with an alkyl or aromatic side group.

heterogeneous presentation of biochemical and biomechanical properties to encapsulated cells. ^{33–38} Additionally, the reversible nature of hydrazone cross-links can lead to erosion of the hydrogel over time, as un-cross-linked polymers diffuse into the surrounding solution, resulting in loss of mass and mechanical stability. ^{24,39,40} To overcome this issue, DCC has been coupled with self-assembling proteins, such as collagen or elastin, that form supramolecular networks. ^{11,41} The structures formed by these self-assembling proteins create a network of secondary cross-links that can minimize erosion and improve hydrogel stability.

Specifically, a recombinant elastin-like protein (ELP) has been used in conjunction with DCC to form stable hydrogels. ELP displays an inverse phase transition and forms protein-rich aggregates above a lower critical solution temperature. 42 This protein aggregation creates a secondary network that stabilizes the DCC hydrogel for extended cell culture. 41 ELPs are highly reproducible and enable intrinsic presentation of biochemical and biomechanical cues through defined sequences of amino acids. 43,44 To create a biomimetic hydrogel, ELP can be combined with recombinant hyaluronic acid (HA), a linear polysaccharide that is broadly expressed in many native tissues. 45,46 Using hydrazone chemistry, hydrogels made of HA and ELP (termed HELP) are stable and have highly tunable biochemical and biomechanical properties. 41,47,48 These HELP materials have been used to successfully culture patient-derived organoids without the need for animal-derived matrices. 49,50

Previous work has reported the injectability of DCC-cross-linked hydrogels, including HELP⁵¹ and polyethylene glycol (PEG)-based systems,⁵² for bioink development and cell delivery applications, respectively. In both material systems, the extrusion of the hydrogel was aided by the incorporation of a small molecule competitor (hydrazinoacetic acid). The

competitor transiently disrupts DCC cross-links, reducing the cross-linking density and increasing extrudability. Postextrusion, the competitor can freely diffuse out of the hydrogel, resulting in a higher cross-linking density and stiffer hydrogel. These proof-of-concept studies demonstrated the utility of a biocompatible competitor to enable extrusion of cell-laden DCC hydrogels. Given the promise of competitors to transiently alter the mechanical properties of DCC hydrogels, we conjectured that the development of a library of competitors would allow us to access a wide range of material properties. Specifically, we hypothesized that competitors with a range of molecular-level properties (e.g., reaction kinetics and thermodynamic constants) would allow us to reproducibly and predictably tune macroscale hydrogel properties (e.g., the gelation time, sol—gel behavior, and gel stiffness).

Toward that goal, here, we identify a library of competitors that display water solubility at physiological conditions and have distinct chemical structures that impact their hydrazone reaction kinetics and thermodynamics. Using models grounded in polymer physics, we relate the molecular-level parameters of the competitors to their effects on the macromolecularnetwork properties to predict the sol-gel phase behavior of HELP hydrogels. We hypothesize that by selecting the appropriate competitor concentration and chemical structure, we can fine-tune the cross-linking density and achieve hydrogels with a wide range of mechanical properties while maintaining a constant polymer concentration. Additionally, to address the rapid gelation of hydrazone-based hydrogels, we take advantage of the transient disruption of cross-links to predictably increase the gelation time, resulting in improved homogeneity of hydrogels. Finally, we demonstrate the usefulness and cell-compatibility of this system by encapsulating patient-derived intestinal stem cells in homogeneous HELP hydrogels to successfully grow human intestinal organoids.

RESULTS AND DISCUSSION

Library of Small Molecule Competitors for DCC Hydrazone Cross-Linking Sites. The formation of a hydrazone bond from aldehyde and hydrazine is facile, reversible, and widely used for cross-linking of dynamic hydrogels (Figure 1A). The reversibility of the reaction is characterized by the forward (k_1) and reverse (k_{-1}) reaction rate constants. The speed of these reactions is governed by the putative rate limiting step of an intermediate aldehyde—hydrazine tetrahedral molecule (Figure S1), which can be stabilized or destabilized by the corresponding side groups (R_1, R_2) . The stability of the hydrazone bond is characterized by the thermodynamic equilibrium constant $K_{\rm eq}$ which is the ratio between k_1 and k_{-1} . As such, $K_{\rm eq}$ can differ over several orders of magnitude, depending on the chemistry of the side groups. The stability of the side groups.

Due to the reversibility of DCC cross-links, at any given time there will be a proportion of aldehydes and hydrazines that remain available and not involved in hydrazone bond formation. We can take advantage of these unreacted cross-linking sites by utilizing diffusible, small molecules that can react with either aldehyde or hydrazine and prevent cross-link formation. By competing for cross-linking sites, the small molecules (termed competitors) reduce the overall cross-link density and hydrogel modulus (Figure 1B). Competitors that reversibly react can be used to transiently disrupt the cross-linking density and then diffuse out of the hydrogel, leading to recovery of the maximum cross-linking density. 51,52

Previously, we have used a hydrazine-based competitor in a recombinant DCC-cross-linked HELP hydrogel. Here, HA and ELP are modified along their backbone with benzaldehyde (HA-BZA; confirmed by NMR, Figure S2) or hydrazine (ELP-HYD; confirmed by NMR, Figure S3), respectively (Figure 1C). Combining the chemically modified HA and ELP results in a hydrazone cross-linked HELP hydrogel that is both biologically active and stable for extended culture. 41,49,50,56 Using this system, we demonstrated the use of hydrazinoacetic acid as a competitor to transiently disrupt cross-linking density for the bioprinting of HELP. S1

Inspired by the use of an alkyl hydrazine competitor to alter hydrogel network properties, we recognized the potential to utilize the side group of the competitor to modulate the reaction kinetics and fine-tune the equilibrium cross-linking density. We hypothesized that by altering the competitor side groups, we could access a broader range of macromolecular network properties and predictably fine-tune hydrogel mechanics. To this end, we identified a library of small molecule competitors that are sufficiently soluble in aqueous solution and contain either aldehyde or hydrazine functionality to react with ELP-HYD or HA-BZA, respectively (Figure 1D). For both the aldehyde and hydrazine functional groups, we selected competitors that contain either an alkyl or an aryl (i.e., aromatic) side group to encompass a broad spectrum of reaction kinetics and equilibrium thermodynamics. Through modulation of these variables, we aim to achieve precise control over the hydrogel properties.

To quantify the extent to which side groups impact reaction parameters, we measured the forward (k_1) and reverse (k_{-1}) reaction rates (Table 1). For these reactions, the complementary reactant was chosen to be either benzaldehyde (BZA) or hydrazinoacetic acid (HydAA), for the hydrazine and aldehyde competitors, respectively. These model reactions

Table 1. Reaction Rates of Competitors with either Benzaldehyde or Hydrazinoacetic Acid^a

Functionality	$k_1 \ (\mathrm{M}^{-1} \ \mathrm{s}^{-1})$	$k_1 \ (\times 10^{-2}) \ (s^{-1})$	$k_{\rm eq}~({ m M}^{-1})$
Aldehyde			
Benzaldehyde ^b (BZA)	0.276 (0.070)	1.71 (0.280)	$1.61 \times 10^3 \\ (0.484 \times 10^3)$
Butyraldehyde (Butanal)	59.9 (5.49)	4.49 (1.07)	1.33×10^{5} (0.34×10^{5})
Hydrazine			
Hydrazinobenzoio acid (HBA)	2.10 (0.40)	1.00 (0.077)	2.09×10^4 (0.43×10^4)
Hydrazinoethanol (HydEtOH)	0.690 (0.301)	1.12 (0.469)	$6.18 \times 10^3 \\ (3.74 \times 10^3)$
$\begin{array}{c} \text{Hydrazinoacetic} \\ \text{acid}^b \text{ (HydAA)} \end{array}$	0.276 (0.070)	1.71 (0.280)	$1.61 \times 10^3 \\ (0.484 \times 10^3)$

"Forward (k_1) and reverse (k_{-1}) reaction rates listed as mean (standard deviation) of N=4 replicates. Reactions were performed in saline solution with equal concentrations (50 μ M) of competitors and model reactants (BZA and HydAA) at 25 °C. Becaute Values of BZA and HydAA.

allow us to directly assess the kinetics between the competitor and the HELP functional groups (HA-BZA and ELP-HYD) without the complexity of the full HA and ELP polymers. This is a strict of the polymers, the use of model molecules establishes the relative reactivity of each small molecule. Hydrazone bond formation was observed by UV spectroscopy and converted to a concentration over time (Figure S4). The reaction rate constants were calculated by fitting to a second order reaction rate, assuming equal concentrations of reactants (Figure S5). S8,60

As expected, we observed that the competitor's side group has a significant impact on reaction rates (k_1, k_{-1}) and product formation (K_{eq}) . Comparing the reaction rates of the aldehyde competitors, we see that the alkyl butyraldehyde (Butanal) has faster reaction rates $(k_1 \sim 60 \text{ M}^{-1} \text{ s}^{-1}, k_{-1} \sim 4 \times 10^{-4} \text{ s}^{-1})$ and a more favored hydrazone production $(K_{\text{eq}} \sim 10^5)$ compared to the aromatic aldehyde (BZA) $(k_1 \sim 0.3 \, \mathrm{M}^{-1} \, \mathrm{s}^{-1}, \, k_{-1} \sim 2 \times 10^{-1})$ 10^{-4} s⁻¹, $K_{eq} \sim 10^3$). When comparing the reaction rates of the hydrazine competitors, the single aromatic hydrazone reactions of BZA, hydrazinoethanol (HydEtOH), and HydAA have similar forward and reverse reaction rates and equilibrium constants $(k_1 \sim 10^{-1}, k_{-1} \sim 10^{-4}, K_{eq} \sim 10^3)$. A double aromatic hydrazone, such as the reaction between BZA and hydrazinobenzoic acid (HBA), resulted in rates that were intermediate between an alkyl and single aromatic hydrazone $(k_1 \sim 2 \text{ M}^{-1} \text{ s}^{-1}, k_{-1} \sim 1 \times 10^{-4} \text{ s}^{-1}, K_{\text{eq}} \sim 10^4)$. These results are consistent with literature, where an alkyl hydrazone (HydAA + Butanal) has the fastest reaction rates and was the most favored reaction compared to the aromatic hydrazone (HydAA + BZA).²⁹ By altering the side groups of the competitors, the equilibrium constant can be tuned over 2 orders of magnitude (10³-10⁵). We rationalized that by utilizing competitors with distinct side groups and reaction parameters, we can achieve distinct reductions in HELP crosslinking density.

Stability of Competitor Reaction Predictably Alters Hydrogel Modulus. To initially assess the impact of a competitor on hydrogel stiffness, we proposed that the effect on cross-linking density will depend upon the relative strength of the two reactions: (1) competitor reaction and (2) cross-linking reaction (Figure 2A). We predicted that as the

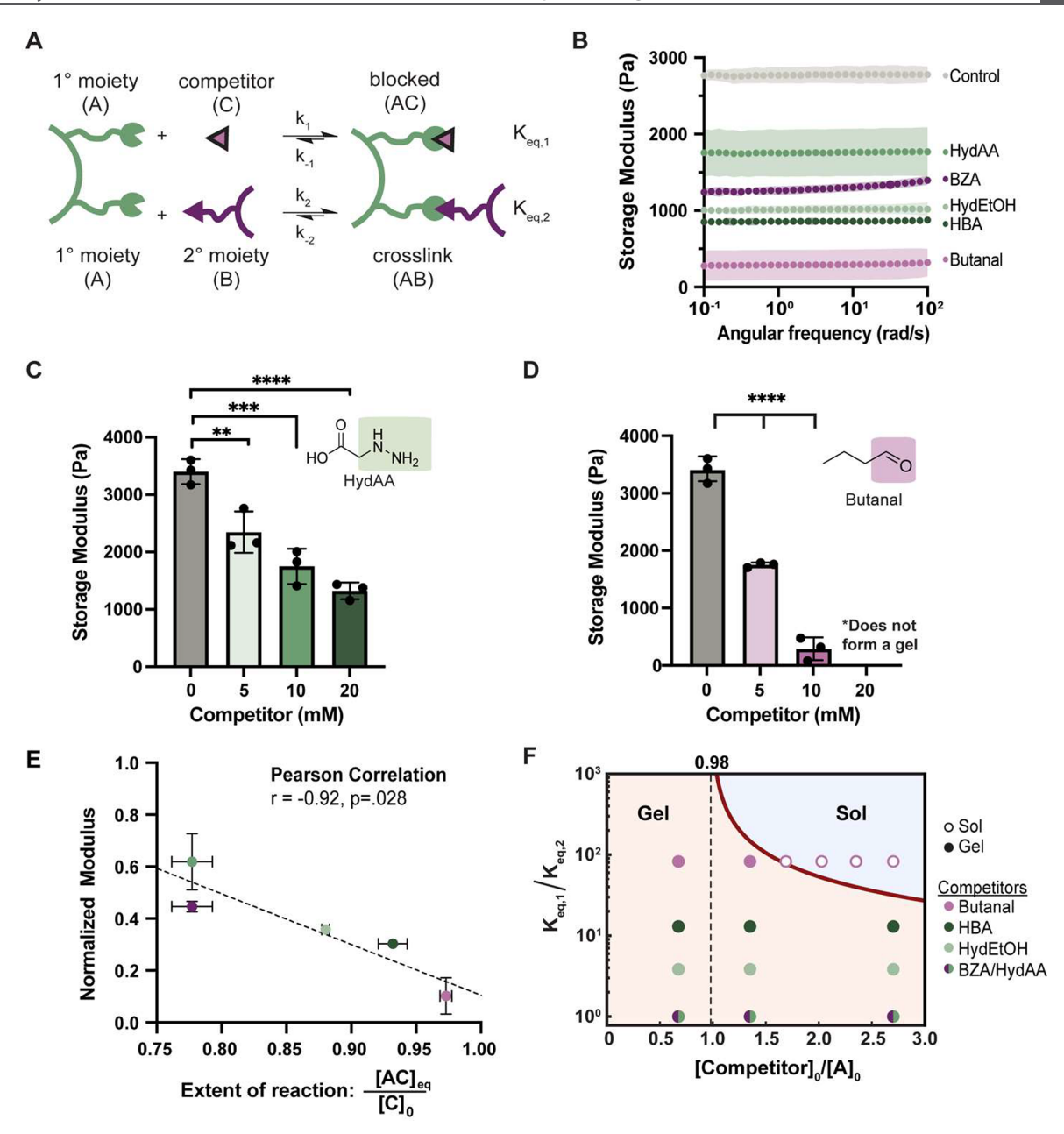


Figure 2. Competitors decrease the stiffness of the HELP hydrogels in a dose-dependent manner. A. Schematic of the two reactions that are simultaneously occurring in a HELP hydrogel with a competitor. The top competitor reaction $(K_{\text{eq},1})$ occurs between the cross-linking moiety (A) and the unbound competitor (C) to form a blocked group (AC) that cannot participate in cross-linking. The bottom cross-linking reaction $(K_{\text{eq},2})$ occurs between the cross-linking moieties of the two polymers, (A) and (B), to form a cross-link (AB). B. A frequency sweep of HELP hydrogels with a 10 mM competitor shows a decrease in the storage modulus. Each point represents an average, and each shaded band represents the standard deviation (N=3). C and D. The addition of either HydAA or Butanal led to a dose-dependent decrease in the storage modulus. Data are mean \pm sd of N=3. Statistical significance was tested by one-way ANOVA with Tukey's multiple comparisons testing: ** = p < 0.001, *** = p < 0.001. E. Correlation of HELP hydrogel storage modulus and equilibrium extent of competitor reaction with Pearson r values reported. Dashed line represents linear regression fit for visualization purposes. F. Predicted sol—gel phase diagram of HELP, depending upon competitor concentration and relative reactivity. Dark red line is the theoretical prediction; points are empirically validated formulations. Open circles are formulations that result in the sol phase. Filled circles are formulations that result in the gel phase. The dashed line shows the ratio of [competitor] $_0/[A]_0$ below which a gel will always form.

equilibrium ratio of the two reactions $(K_{\rm eq,1}/K_{\rm eq,2})$ increases, there will be a greater disruption of cross-links and a lower gel stiffness. To validate this, we empirically determined the impact of competitor $K_{\rm eq}$ on the modulus of HELP formed from precursor solutions of HA-BZA and ELP-HYD at a 1:1 BZA to HYD ratio. To minimize off-target reactions, competitors were added to the precursor solution that had

the same functionality, i.e., hydrazine competitors were added to ELP-HYD, and aldehyde competitors were added to HA-BZA. At 10 mM of competitor, which represents a ratio of 4:3 of competitor to cross-linking sites, all competitors led to a significant decrease in the HELP modulus compared to the 0 mM control (Figure 2B). Based upon our hypothesis that the relative strength of the reactions will dictate cross-linking

disruption, we expected to see a decreasing trend in modulus for HELP formulations with competitors resulting in an aromatic hydrazone ($K_{\rm eq,1}/K_{\rm eq,2}\sim 10^{\circ}$), double aromatic hydrazone ($K_{\rm eq,1}/K_{\rm eq,2}\sim 10^{1}$), and alkyl hydrazone ($K_{\rm eq,1}/K_{\rm eq,2}\sim 10^{1}$). Consistent with our prediction, the least favored competitor reaction (HydAA: $K_{\rm eq,1}/K_{\rm eq,2}\sim 10^{\circ}$) had the least impact on modulus (1.75 \pm 0.3 kPa) compared to the control (2.83 \pm 0.13 kPa); whereas the most favored competitor reaction (Butanal: $K_{\rm eq,1}/K_{\rm eq,2}\sim 10^{2}$) had the largest drop in modulus (0.29 \pm 0.2 kPa).

We next examined the effect of competitor concentration on the hydrogel modulus. As expected, the modulus has a dose-dependent response, with an increasing competitor concentration leading to further gel weakening. To examine this dose-dependent response, we selected the competitors with the lowest $K_{\rm eq}$ (HydAA, aromatic hydrazone) and the highest $K_{\rm eq}$ (Butanal, alkyl hydrazone). Increasing the concentration of HydAA from 5 to 10 and 20 mM reduced the gel modulus from 2.3 \pm 0.4 to 1.8 \pm 0.3, and 1.3 \pm 0.1 kPa, respectively (Figure 2C). We observed a similar response with Butanal; as we increased the concentration from 5 to 10 mM, the gel modulus decreased from 1.8 \pm 0.2 to 0.3 \pm 0.2 kPa (Figure 2D). Further increasing the concentration of Butanal to 20 mM resulted in even greater inhibition of cross-linking and the inability to form a gel.

As a first approximation of the impact of the competitor K_{eq} on the hydrogel modulus, we predicted the percentage of competitors that would be bound to the biopolymer at equilibrium. Using the reaction kinetic parameters from 1 we calculated the extent of hydrazone formation in the competitor reaction at equilibrium ($[AC]_{eq}/[C]_0$). Comparing the extent of competitor reaction to the hydrogel modulus, we see that the level of modulus decrease is strongly linearly correlated (r = -0.92) (Figure 2E). This demonstrates that as the competitor hydrazone bond becomes more favored (higher $K_{\rm eq}$), the modulus of the hydrogel continues to decrease. Notably, the hydrazone bond prediction uses only the competitor reaction and does not take into account the cross-linking reaction. Additionally, the reaction studies were performed on model molecules without considering the effect of the polymer backbone and reduced diffusion. Thus, while this analysis cannot predict the absolute modulus, 57 it can be used to predict the relative change in modulus. Using simple thermodynamic arguments, we can predict that in our HELP system, an alkyl aldehyde competitor, such as Butanal, will lead to a significantly greater decrease in modulus, compared to an alkyl hydrazine competitor, such as HydAA, leading to a 0.1and 0.6-fold change in modulus, respectively (Figure S6).

In addition to predicting the change in gel stiffness, we also wanted to predict the limits of competitor reactivity ($K_{\rm eq}$) and concentration that would still allow for hydrogel formation. A gel is formed when sufficient cross-linking sites have reacted to form a percolating network (i.e., infinite polymer).⁶¹ In a mean-field description of gel formation, the gelation point occurs when the cross-linking has proceeded to a critical extent of reaction (p_c) to form a percolated network.⁶² Reactions that have not reached p_c are in the sol phase, while those that are at or above p_c are in a gel phase. We hypothesized that we could use this theoretical framework to predict which competitor formulations do not achieve HELP gelation. Using percolation theory, we assembled a phase diagram to delineate combinations of relative reaction strength and competitor concentration that produce a gel or sol. Here we use a classical

model of sol–gel phase transition based on percolation of cross-links on a fractal, Bethe lattice. First, we used the kinetic rate law equations for the two competing competitor and cross-linking reactions (Figure 2A) to relate the relative strength of the reactions ($K_{\rm eq,1}/K_{\rm eq,2}$) and initial concentration of the reactants ($[A]_0$, $[B]_0$, $[C]_0$) to the extent of cross-linking reaction (p; see Method S1 for full derivation):

$$\frac{K_{\text{eq,1}}}{K_{\text{eq,2}}} = \frac{\left([A]_0 - \frac{p}{K_{\text{eq,2}}(1-p)} - p[B]_0 \right) (1-p)}{\left([C]_0 - \left([A]_0 - \frac{p}{K_{\text{eq,2}}(1-p)} - p[B]_0 \right) \right) p} \tag{1}$$

Then, to determine the critical extent of reaction, we employ mean-field theory to express p_c in terms of the polymer functionality f (i.e., the number of potential cross-linking sites on the polymer) 61,63,64 as

$$p_{c} = \frac{1}{f - 1} \tag{2}$$

The high functionality of the HELP system, taken as the average functionality of HA-BZA (f=102.8) and ELP-HYD (f=12.6), leads to a small critical extent of reaction ($p_c=0.018$). This represents a lower limit, as the Bethe model of percolation does not take into account the formation of network defects, such as loops. Nevertheless, the implication of such a highly functionalized system is that even when many of the polymer reactive sites are blocked with a competitor, the system is still predicted to form a gel (Figure 2F). Using the simplifying assumptions of the Bethe model, we calculated that as long as the competitor concentration is 98% of the potential cross-linking sites or less ($[C]_0/[A]_0 < 0.98$), there will be sufficient cross-linking to form a percolated network (i.e., gel) at equilibrium (Method S1).

Combining eqs 1 and 2, we assembled a sol-gel phase diagram that identifies competitor conditions that enable gel formation for the HELP system (Figure 2F, solid line). Inputting the reaction parameters for each of the competitors, we predicted whether different formulations with varying competitor concentrations would form a sol or gel phase. For the competitor Butanal, which has a high $K_{\rm eq}$, a competitor concentration ~1.7-times the concentration of cross-linking sites results in a system that will not gel. This predicted behavior is validated by the inhibition of HELP gelation at a Butanal concentration of 12.5, 15, 17.5, and 20 mM (corresponding to ~ 1.7 , ~ 2 , ~ 2.4 , and ~ 2.7 -times the concentration of cross-linking sites, respectively). In contrast, a Butanal concentration of 10 mM (1.35 times the concentration of cross-linking sites) is accurately predicted to form a HELP gel. Thus, by combining reaction kinetics with the percolation theory of gelation, we can predict the concentration of competitors that will prevent gelation from

By selecting competitors of appropriate concentration and reactivity, we can access a range of physiologically relevant stiffness for biomimetic studies of soft tissues. The phase space of possible hydrogel moduli is set by the range of possible competitor concentrations and $K_{\rm eq}$. The maximum gel stiffness is achieved when no competitor is present. The minimum gel stiffness possible is achieved when the competitor is just below the critical concentration that prevents the formation of a percolated network. Between these two values, the entire phase

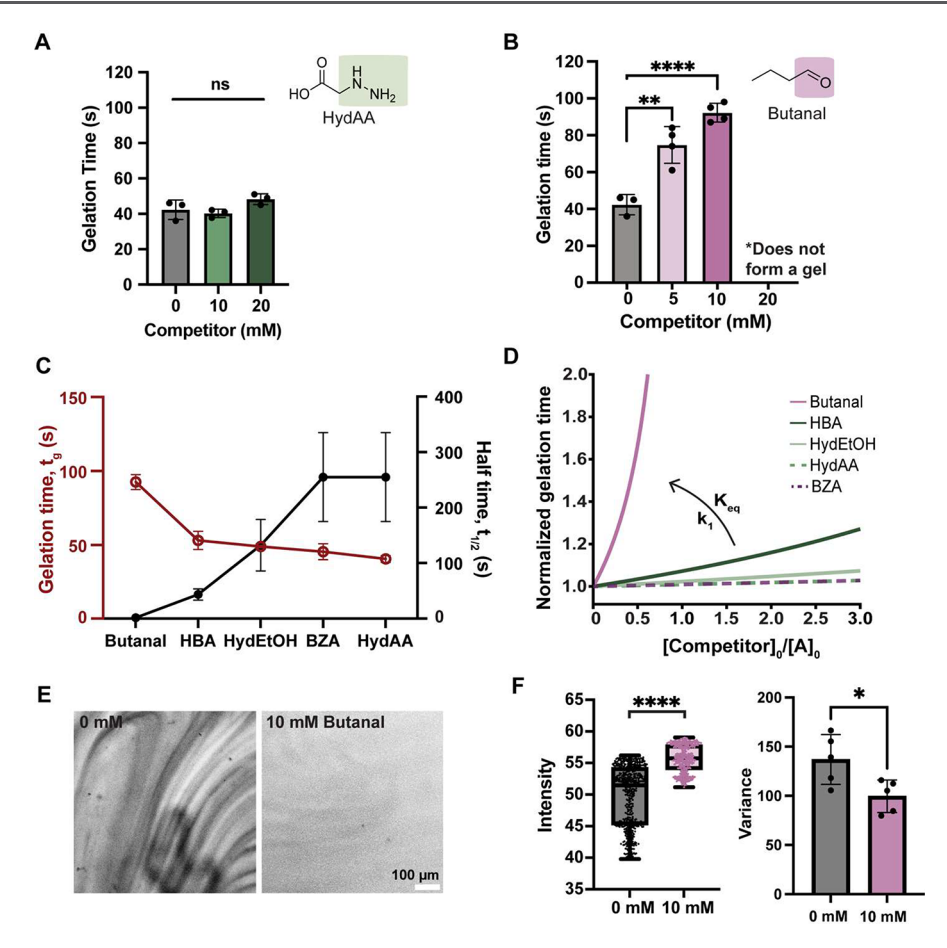


Figure 3. Competitors can modulate the gelation time and improve the hydrogel uniformity. A. HydAA does not significantly alter the gelation time of the HELP hydrogels over a range of concentrations. B. Butanal significantly increases the gelation time in a dose-dependent manner. Data shown are mean \pm sd of N = 3-4. Statistical significance was tested by one-way ANOVA with Tukey's multiple comparisons testing: ** = p < 0.01, **** = p < 0.0001. C. Experimental gelation time (left axis, open circles) and competitor reaction half-time (right axis, closed circles) show an inverse relationship for the families of different competitors. D. Predicted gelation time normalized to gelation time of formulation without a competitor for varying competitor concentrations. E. Representative fluorescent images of HELP with or without 10 mM Butanal and rhodamine B dye added to visualize hydrogel homogeneity. F. Quantification of HELP hydrogel homogeneity. Left: Pixel intensity of fluorescent images. Right: Quantified pixel intensity variance. Data shown are mean \pm sd of N = 5. Unpaired two tailed Student's t test; * = p < 0.05, **** = p < 0.0001.

space of possible moduli can be accessed in a continuous manner by simply changing the competitor concentration.

Tuning HELP Gelation Time by Tuning Competitor Reactivity. We next addressed the rapid gelation of hydrazone-cross-linked DCC hydrogels, which can result in heterogeneous presentation of biochemical and biomechanical material properties. Based upon the predicted and observed effects of the competitor on hydrogel stiffness, we reasoned that transient disruption of cross-linking would also alter gelation kinetics. As expected, addition of a competitor with appropriate reaction kinetics can delay the time required to reach a percolated polymer network in a dose-dependent manner (Figure 3). For a relatively slow reacting competitor (HydAA, $k_1 \sim 10^{-1} \text{ M}^{-1} \text{ s}^{-1}$, $K_{\rm eq} \sim 10^3$), addition of a high concentration (20 mM) did not significantly impact gelation time ($t_g \sim 45$ s), even though it weakened the hydrogel modulus from ~3 to 1.3 kPa. (Figure 3A). Comparatively, a rapidly reacting competitor (Butanal, $k_1 \sim 10^1 \ \mathrm{M}^{-1} \ \mathrm{s}^{-1}$, $K_{\mathrm{eq}} \sim$ 10^{5}) significantly increased the gelation time from ~45 to ~75 and ~95 s with increasing concentrations of 0, 5, and 10 mM, respectively (Figure 3B). The difference in gelation times can be attributed to the difference in forward reaction rate and equilibrium constants of the competitors, which both differ

over 2 orders of magnitude between Butanal and HydAA. This is advantageous, as 5 mM Butanal and 10 mM HydAA both led to a decrease in modulus from ~ 3 to ~ 1.75 kPa; however, 5 mM Butanal increased the gelation time by ~ 1.7 fold while HydAA did not significantly impact gelation. Excitingly, this demonstrates that by altering competitor kinetics and concentration, we can independently tune the hydrogel gelation time and the final hydrogel modulus, which allows for gel optimization for different applications.

We next sought to predict the macroscale gelation time using the experimentally measured molecular-level kinetic parameters (Table 1). Using the kinetic reaction parameters, we calculated the theoretical half-time $(t_{1/2})$ to reach equilibrium of the competitor reaction at a concentration of 10 mM, assuming a well-mixed reaction (Figure 3C). The BZA and HydAA reactions are predicted to take the longest time to reach equilibrium $(t_{1/2}=254\pm80~{\rm s})$ compared to the relatively fast Butanal reaction $(t_{1/2}=1.59\pm0.14~{\rm s})$. We rationalized that competitors with rapid reaction times would result in the slowest gelation times, since the competitor can rapidly react with the cross-linking sites, preventing them from participating in gelation. This prediction was validated by experimentally measuring the hydrogel gelation time for each

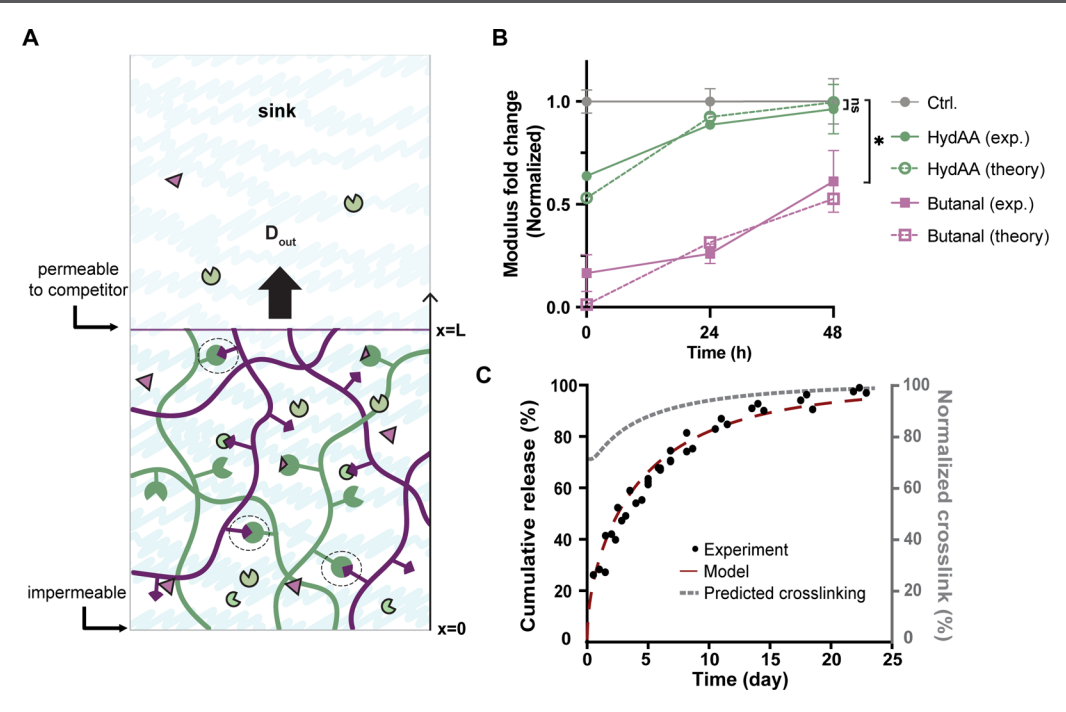


Figure 4. Temporal release of competitors from HELP. **A.** Schematic of competitor release from HELP into the surrounding infinite sink of medium. **B.** Modulus recovery of HELP after competitor release over 48 h. HELP formulations with 10 mM HydAA show rapid recovery, while formulations with 10 mM Butanal show a slower recovery. Data are mean \pm sd of N=3. Statistical significance was tested by one-way ANOVA with Tukey's multiple comparisons testing: * = p < 0.05, n.s. = not significant. **C.** Theoretically predicted (red dashed line) and experimentally measured (dots) cumulative release of 2.8 mM Butanal along with theoretically predicted percentage of hydrazone cross-links formed over 21 days (gray dashed line).

of the competitors by using oscillatory rheology. Consistent with our hypothesis, we observed a qualitative inverse relationship, where faster competitor reactions (smaller $t_{1/2}$) resulted in slower gelation times (larger t_{σ}).

To build a more detailed predictive model of gelation time, we used the kinetic reaction parameters to estimate the time required to form the percolation threshold number of crosslinks (p_c) for any concentration of competitor. Specifically, Matlab was used to numerically solve a system of two coupledreaction equations: (1) the reaction between the two crosslinking functional groups and (2) the reaction between the competitor and the complementary functional group. The calculated gelation time shows a clear dependence on the competitor forward reaction rate and $K_{\rm eq}$ (Figure 3D). This model also explains why the empirically observed gelation time of HELP is increased with Butanal but is not significantly increased with HydAA. The addition of HydAA up to 20 mM $(\sim 2.5 \text{ [competitor]}_0/[A]_0)$ has a negligible effect on the gelation time both theoretically (Figure 3D) and experimentally (Figure 3A,C). Meanwhile, Butanal reacts significantly faster and asymptotically approaches an infinite gelation time, which agrees with our experimental data (Figures 2C and 3B) and the theoretical prediction that Butanal prevents gelation at higher concentrations (Figure 2F).

We proposed that by using a competitor to increase gelation time, we could overcome the challenge of fabricating homogeneous, hydrazone-cross-linked HELP, by enabling more time for mixing prior to the onset of gelation. We visualized the macroscopic structure of a stiff HELP formulation (~3 kPa) with and without Butanal by adding a soluble fluorescent Rhodamine B dye to the ELP component prior to mixing. Without a competitor, the hydrogel rapidly gelled, resulting in a heterogeneous hydrogel with nonuniform

distribution of polymer and dye (Figure 3E). However, addition of 10 mM Butanal allowed for adequate mixing of the polymers and formation of a homogeneous hydrogel. To quantitatively evaluate the heterogeneity of HELP hydrogels with or without a competitor, we compared the spatial distribution of the fluorescent signal. Compared to the rapidly gelling control, the increased gelation time of HELP with Butanal produced a significantly narrower distribution of fluorescence intensity, with a significantly lower variance compared to the rapidly gelling condition (Figure 3F, Figure S7). By using a rapidly reacting competitor to slow down gelation kinetics, we demonstrated the ability to produce uniform HELP hydrogels, even for fast cross-linking reactions.

Diffusion and Release of Competitor from the Hydrogel System. An advantage of using reversible small molecules as competitors is their ability to diffuse out of the system. After gelation, the competitor can diffuse away from the hydrogel to recover the equilibrium density of cross-links between the polymers, which results in hydrogel stiffening over time (Figure 4A). The rate at which competitors diffuse out of the hydrogel depends upon the competitor diffusivity and the stability of the hydrazone bond, which can be predicted by the K_{eq} of the competitor. Comparing competitors with low and high K_{eq} demonstrates the range of time scales over which the competitors can diffuse out of the gel. For a low K_{eq} (HydAA, $K_{\rm eq} \sim 10^3$), the modulus recovers by 89% over 24 h and fully recovers after 48 h, whereas a higher $K_{\rm eq}$ (Butanal, $K_{\rm eq} \sim 10^{\rm s}$) induces a significantly slower recovery, with 61% of the maximum modulus recovered by 48 h (Figure 4B, filled circles). By using a competitor that can delay gelation and then diffuse out of the hydrogel, we can produce a DCC-crosslinked hydrogel that is homogeneous and stiff (Figure 3E, Figure 4B). This is often challenging for hydrazone-cross-

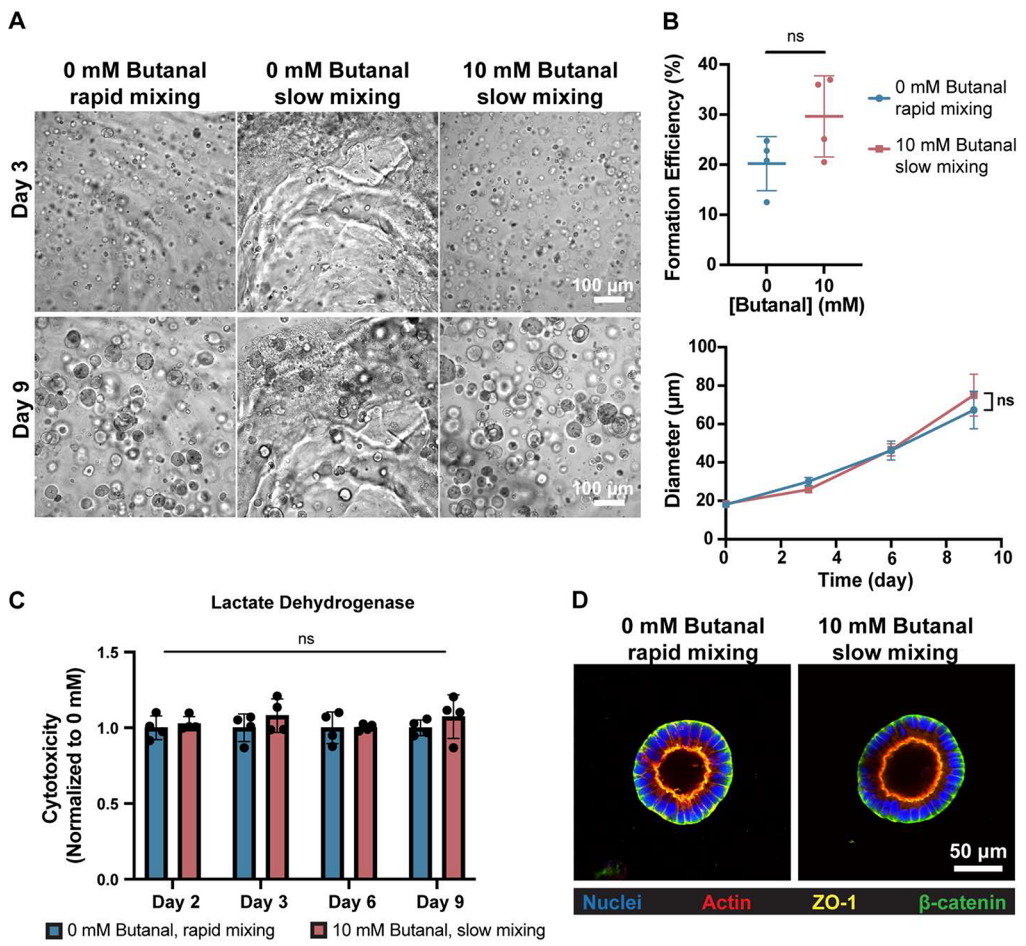


Figure 5. Intestinal organoid culture in HELP with competitor.

Figure 5. Intestinal organoid culture in HELP with competitor. **A.** Representative bright-field images of intestinal organoids at day 3 (top) and day 9 (bottom) in rapidly gelling HELP (0 mM Butanal), mixed slowly; and slowly gelling HELP (10 mM Butanal), mixed slowly. **B.** Organoid formation efficiency on day 3 (top) and growth rate through day 9 (bottom) for intestinal organoids grown from single cells. Data shown are mean \pm sd of n = 60 per gel, N = 4 gels. Unpaired, two tailed Student's t test; n.s. = not significant. **C.** Lactate dehydrogenase (LDH) cytotoxicity assay on intestinal organoids in HELP with 0 or 10 mM Butanal. At each time point, cytotoxicity percentage is normalized to 0 mM control. Data shown are mean \pm sd of N = 4. Two-way ANOVA with Tukey multiple comparisons testing; n.s. = not significant. **D.** Confocal fluorescence of polarized intestinal organoid morphology at day 9 in HELP with 0 or 10 mM Butanal.

linked systems, as stiffer gels require a higher concentration of cross-linking functional groups, which leads to more rapid gelation and a higher likelihood for inhomogeneity.

The rate at which the stiffness increases is dependent on the competitor reaction parameters and diffusivity. To predict the rate at which the hydrogel stiffness recovers, we assembled a series of reaction-diffusion differential equations to describe the system. Taking advantage of the symmetry of the hydrogel, the model was simplified to a 1-dimensional system and the boundary conditions were set by the impermeable culture plate at the bottom of the hydrogel and the sink of competitor-free solution at the top (Figure 4A, Method S2). The diffusivity of the freely diffusing small molecule competitor was estimated by a linear extrapolation of diffusion rates of FITC-dextran probes, measured by Fluorescence Recovery After Photobleaching (FRAP, Figure S8). To experimentally validate this theoretical model, an aldehyde-modified Rhodamine B (aldrho) was incorporated into HELP (2.8 mM ald-rho). This boundary condition can be approximated as an infinite sink due to the high sink:gel volume ratio (100:1) and the daily media replacements. Using Matlab, we numerically solved the system of equations and compared the predictions with the

experimentally observed release profile of ald-rho, which displays a sustained cumulative release over a period of 3 weeks (Figure 4C, red dashed line and black dots). Both the shape and time scale of the experimentally observed release profile matched the theoretical predictions. Using the release model, we can predict both the concentration of competitor remaining in the gel and the concentration of cross-links over time. We normalized the concentration of cross-links to the theoretical maximum concentration of cross-links in a HELP system with no competitor. This provides a method by which cross-linking density over time can be predicted using the reaction kinetic parameters of candidate competitors (Figure 4C, gray dashed line).

Applying this reaction-diffusion approach, we predicted the modulus recovery for HELP formulations with 10 mM either HydAA or Butanal (Figure 4B, open circles). We adjusted the boundary condition of the coupled reaction-diffusion model to better replicate tissue culture conditions (sink to gel volume ratio of 20:1) and account for the accumulation of the competitor into a finite volume of solution. Using Matlab, we found excellent agreement between the experimentally determined and theoretically predicted values for both

HydAA and Butanal competitors, validating this model for the prediction of macromolecular network properties using molecular parameters.

Competitor Compatibility with Human Intestinal Organoid Culture. A key requirement of a competitor for in vitro culture is that it must be cell compatible. To explore the impact of a competitor on the growth and morphology of cells, we grew patient-derived intestinal organoids from single stem cells in the presence or absence of Butanal. Several synthetic matrices have been reported for the culture of intestinal organoids, demonstrating that these cultures are sensitive to both the matrix stiffness and the concentration of incorporated integrin-binding ligands. 65-70 We have previously demonstrated the formation and growth of adult human intestinal organoids in HELP formulations without any competitors. 49 Here we evaluated human intestinal organoid growth in HELP gels formulated with and without 10 mM Butanal, which led to the largest increase in gelation time and homogeneous mixing of gel precursors (Figure 3B,E). The competitor was added only at the time of encapsulation, which allows the Butanal to diffuse out of the gel over time. Both gels were formulated to include 1 mM RGD ligand and a final shear modulus of 3 kPa.

To demonstrate the usefulness of delayed gelation, we prepared a series of three HELP formulations: (i) a rapidly gelling HELP without a competitor present (~45 s gel time) that was mixed very rapidly (<10 s) to allow for homogeneous mixing prior to gelation, (ii) a rapidly gelling HELP without a competitor present (~45 s gel time) that was mixed more slowly (~30 s), and (iii) a slowly gelling HELP with 10 mM Butanal competitor (~95 s gel time) that was mixed slowly (~30 s). All three HELP formulations had identical concentrations of HA and ELP. Consistent with the results in Figure 3E,F, when the rapidly gelling HELP was mixed more slowly, the resulting gel was heterogeneous, leading to separation of the material (cloudy and disordered; Figure 5A). Over 9 days of culture, the cells in this inhomogeneous gel formed organoids of variable morphology and size and frequently grew in clumps (Figure 5A, Figure S9). In contrast, we saw robust and reproducible formation of a homogeneous culture of spherical intestinal organoids under the other two HELP conditions: rapidly mixed HELP with 0 mM Butanal (i.e., rapid gelling) and slowly mixed HELP with 10 mM Butanal (i.e., slow gelling) (Figure 5A). The ability to achieve homogeneous cell encapsulation with prolonged mixing times is technically advantageous, especially for studies with a high number of technical replicates where manual rapid mixing of multiple gels is cumbersome.

To evaluate the potential cellular effects of Butanal, we quantified the percentage of single cells that were capable of forming organoids (i.e., formation efficiency at day 3) and the organoid growth rate (i.e., organoid diameter over 9 days) in rapidly gelling HELP and slow gelling HELP, containing 0 or 10 mM Butanal, respectively. The presence of Butanal resulted in no significant differences in formation efficiency (Figure 5B, top) and growth rate (Figure 5B, bottom) compared to the 0 mM control, which suggests a negligible impact of the competitor on stem cell culture. To determine whether Butanal had any measurable cytotoxic effects, we measured lactase dehydrogenase (LDH), an extracellular metric of cytotoxicity. We observed no significant difference in cytotoxicity across both conditions throughout the entire 9 day culture period (Figure 5C). Over this time period, these

cells formed early organoid structures (often termed enteroids in the intestinal organoid literature) with a polarized epithelial lumen, demonstrated by localization of the tight junction protein (zonal occludens-1, ZO-1) and adherens junction protein (β -catenin) to the apical and basal sides, respectively (Figure 5D). Importantly, the presence of 10 mM Butanal did not lead to any aberrant morphology. Furthermore, we also demonstrated that Butanal is a cell-compatible competitor for human intestinal organoid growth and culture in HELP formulations with higher ligand concentrations (2 mM RGD, Figure S10). Thus, using human intestinal organoids as a test case, we have demonstrated that the competitor Butanal is a cell compatible small molecule that can be successfully used in the formulation of DCC-cross-linked hydrogels for cell culture applications.

CONCLUSION

Using a library of competitors that transiently disrupt formation of cross-links in a DCC-based hydrogel, we establish a framework to connect molecular-level properties to macromolecular network properties in a recombinant HELP hydrogel. We showed that by altering the chemical structure and incorporating either alkyl or aryl side groups, we can tune the competitor reaction parameters over 2 orders of magnitude. With this library, we successfully disrupted the formation of hydrazone cross-links and observed a decrease in the stiffness of the hydrogel. The reduction in the hydrogel stiffness was directly correlated to the thermodynamic equilibrium properties of the competitor reaction. Previously published work comparing the kinetics of benzaldehyde vs aldehyde reactive groups on resulting hydrogel mechanical properties were consistent across several different polymer systems (polyethylene glycol, 58 hyaluronic acid-only, 39' and elastin-like protein/hyaluronic acid^{41,56}), suggesting that our library of competitors may also be translated to other polymeric materials.

By employing a model rooted in percolation theory, we identified the lower and upper limits of competitor reactivity and concentration that allow for gel formation. Similarly, we empirically showed that the competitor could delay the onset of a fully percolated network, thereby increasing the gelation time of the system. Using a combination of kinetic and thermodynamic equilibrium approaches, we predicted the gelation time of the HELP formulations with the competitor. Furthermore, an advantage of a small molecule competitor that reacts reversibly is its diffusion out of the system over time, leading to a recovery of the equilibrium number of cross-links in the hydrogel. The diffusion and recovery of cross-links depend on the reaction parameters of the competitor and were predicted and validated using a coupled reaction-diffusion model.

Overall, we demonstrated the cell compatibility of Butanal as a competitor for the encapsulation and culture of stem-cell-derived human intestinal organoids. When cultured in the more homogeneous gels, the intestinal organoids were more spherical and evenly dispersed. In the future, the gelation time in the presence of a competitor could be further increased to allow for serial robotic pipetting, which would improve the scalability of human intestinal organoid cultures. In addition, this approach can be expanded to other biological systems to reproducibly create homogeneous hydrogels for tissue engineering applications. As with other common cross-linking schemes, hydrazine and aldehyde reactive groups are known to

cross-react with other biochemical compounds. ^{54,75} Therefore, in the future, similar predictive models could be developed to estimate the degree and rate of off-target reactions with other biomolecules.

By using simple models, we accurately predicted complex macromolecular network properties, including the kinetics and formation of a percolated network (i.e., gelation time and phase diagram, respectively). However, it is important to note that the underlying assumptions in the model require a completely defect-free system with independent probabilities of bonding. Although this was sufficient for our linear biopolymers, future work will generalize these models to encompass more complex geometries, including branched polymers (e.g., 4-arm PEG). The model could further be improved by accounting for polymer diffusion; this would be a required component to predict hydrogel erosion time, which is a common concern for hydrogels composed of dynamic crosslinks. 24,39,40 Additionally, employing finite element analysis can enhance the precision in predicting local gradients in competitor concentration and time-dependent hydrogel properties. Moving forward, the models developed herein will enable a prirori design of competitors for highly specified hydrogel gelation kinetics and mechanics.

■ EXPERIMENTAL SECTION

Library of Small Molecule Competitors. Unless otherwise stated, all small molecule competitors in this study were purchased from Sigma: Hydrazinoacetic acid (HydAA, 14150-64-2, BOC Sciences), Hydrazinoethanol (HydEtOH, 54340), Hydrazinobenzoic acid (HBA, 246395), Butyraldehyde (Butanal, 538191), and Benzaldehyde (BZA, B1334).

Synthesis of HA-Benzaldehyde. Hyaluronic acid (HA) was modified following previously reported protocols. First, an alkyne group was appended onto HA (100 kDa, sodium salt, LifeCore Biomedical HA100 K). HA was dissolved in 2-(N-Morpholino) ethanesulfonic acid (MES) buffer (0.2 M MES hydrate (Sigma M2933), 0.15 M NaCl in Milli-Q water; pH 4.5) at a concentration of 1 wt %. Propargylamine (Sigma P50900) was added to the solution (6 equiv per HA carboxylic acid group), and the pH was adjusted to 6 using NaOH. N-Hydroxysuccinimide (NHS; 6 equiv:HA carboxylic acid group; Thermo Fisher 24500) and EDC (6 equiv:HA carboxylic acid group; Thermo Fisher 22980) were added sequentially, and the reaction was stirred continually for 24 h. After the reaction, the solution was dialyzed against Milli-Q water for 3 days using 10 kDa MWCO dialysis tubing (Spectrum Laboratories). The solution was then sterile-filtered and lyophilized.

Benzaldehyde-modified HA was prepared from HA-alkyne via a copper click reaction with azido-benzaldehyde (synthesized using a previously reported protocol⁵⁰). All solutions used for the copper click reaction were degassed for 30 min under nitrogen. The lyophilized HA-alkyne product was dissolved at a 1 wt % concentration in isotonic 10x phosphate buffered saline solution (10× PBS; 81 mM sodium phosphate dibasic, 19 mM sodium phosphate monobasic, 60 mM sodium chloride in Milli-Q water; pH 7.4) supplemented with 1 mg/mL beta-cyclodextrin (Sigma C4767). Solutions of 4.52 mM sodium ascorbate (0.18 eq:HA carboxylic acid groups, Sigma A7631) and 0.24 mM copper(II) sulfate pentahydrate (0.0096 eq:HA carboxylic acid groups, Sigma 209198) dissolved in Milli-Q water were sequentially added to the HA-alkyne reaction for a final concentration of 452 and 24 μ M, respectively. Finally, a solution of azidobenzaldehyde (2.0 equiv:alkyne groups) dissolved in a minimal amount of anhydrous DMSO (~300 mg/mL; Sigma 276855) was added to the reaction, and the final solution degassed for 10 min. The reaction was allowed to proceed for 24 h under constant stirring. Following the reaction, an equal volume of 50 mM ethylenediaminetetraacetic acid disodium salt dihydrate (EDTA, Fisher O2793-500) at pH 7.0 was added to chelate the copper

and stop the reaction. The solution was then dialyzed, filtered, lyophilized, and stored at $-20~^{\circ}\text{C}$ as previously described. The degree of modification of HA-benzaldehyde was calculated via nuclear magnetic resonance spectroscopy (^{1}H NMR, D₂O; Figure S3). ^{1}H NMR (500 MHz, D₂O) δ ppm 9.9 (1H, aldehyde); 7.93 and 7.82 (2H each; benzene ring); 7.9 (1H, triazole link); 1.8 (3H, HA acetyl group, reference).

Synthesis of ELP-Hydrazine. Elastin-like Protein Expression. Elastin-like protein (ELP) was produced as previously described.⁴⁴ In brief, pET15b plasmids encoding the ELP sequence (Figure S2) were transformed into BL21(DE3) pLysS Escherichia coli (Invitrogen C606003). The bacteria were cultured in Terrific Broth (Thermo Fisher H26824.36) at 37 $^{\circ}$ C until an OD₆₀₀ of 0.8, at which point ELP expression was induced by the addition of 1 mM isopropyl β -D-1thiogalactopyranoside (Thermo Fisher BP1755). After an expression period of 7 h, the bacteria were pelleted and resuspended in a TEN Buffer (10 mM Tris (Fisher BP152-1), 1 mM EDTA (Fisher BP2482100), and 100 mM NaCl (Fisher BP358-212), pH 8.0) containing 10 µM DNase I (Sigma DN25) and 1 mM phenylmethanesulfonyl fluoride (PMSF; MP Biomedicals 195381) protease inhibitor. ELP was recovered from the bacteria pellet by three freezethaw cycles and repeated cold (4 °C) and hot (37 °C) spin thermocycling and centrifugation steps. This was followed by 3 days of dialysis against Milli-Q water at 4 °C using 10 kDa MWCO dialysis tubing (Spectrum Laboratories). The purified ELP product was then lyophilized and stored at -20 °C.

Synthesis of Hydrazine-Modified Elastin-like Protein. The amine groups on lysine present in ELP were modified following previously reported protocols. 48,49 Lyophilized ELP was dissolved in equal volumes of anhydrous dimethyl sulfoxide (DMSO; Sigma 276855) and anhydrous dimethylformamide (DMF; Sigma 227056) to a final solution of 3% ELP (w/v). In a separate vessel, tri-Boc hydrazinoacetic acid (2 molar equivalence per ELP amine; Sigma 68972) was dissolved in DMF at 2.1% (w/v). Once dissolved, tri-Boc hydrazinoacetic acid was activated by the addition of hexafluorophosphate azabenzotriazole tetramethyl uronium (HATU; 2 equiv per amine; Sigma 445460) and 4-methylmorpholine (5 equiv per amine; Sigma M56557). After 10 min, the activated tri-Boc hydrazinoacetic acid was added dropwise to the ELP solution under continuous stirring and allowed to react for 24 h at RT. The modified ELP was then precipitated out by dropwise addition of the reaction solution to icecold diethyl ether (Fisher E138) and collected by centrifugation (18,000g, 25 min). The product was dried overnight under nitrogen. The degree of modification (Figure S2) was measured in a 10 mg/mL solution of modified-ELP in DMSO-d6 via 1 H NMR (δ ppm 7.00 and 6.62 (2H each, tyrosine amino acid); 1.46 and 1.39 (27H, Boc groups); 500 MHz, Varian Inova). The Boc protecting groups were removed by dissolving the modified-ELP in a 1:1 solution of (DCM; Sigma DX0835-3) and trifluoroacetic acid (TFA; Sigma T6508) supplemented with 5% v/v tri-isopropylsilane (Sigma 233781) to a final concentration of 3.3% ELP (w/v). The deprotection reaction proceeded for 4 h under continuous stirring. The final ELP-hydrazine was then precipitated out, centrifuged, dried, and resuspended in water prior to dialysis following the above protocol. The dialyzed product was then sterile-filtered and lyophilized, producing a white solid, which was stored at -20 °C.

Reaction Kinetic Studies and Modeling. All reaction kinetic studies were performed using a UV—vis plate reader (BioTek Synergy H1) in 96-well UV transparent well plates (Corning 3635). For all experiments, a blank was subtracted from the absorbance prior to analysis. The blank was defined as a condition with only the model molecule (BZA or HydAA) present. All samples and blanks were performed in triplicate (n = 3).

To determine the wavelength of hydrazone absorbance, the concentration of the competitor was varied from 0, 1, 10, and 100 μ M and the concentration of the model molecule (BZA or HydAA) was held constant and sufficiently high (1 mM) to drive the competitor reaction to completion. The spectra (240–550 nm) were recorded and the wavelength with the largest increase with concentration was defined as the peak absorbance wavelength ($\lambda_{\rm Butanal}$

= 240, $\lambda_{\rm HydAA,HydEtOH}$ = 280, $\lambda_{\rm HBA}$ = 350 nm). Following the Beer–Lambert Law, ⁷⁶ the molar extinction coefficient, ε , a proportionality constant that relates absorbance to concentration of the compound was determined by the slope of a linear fit of absorbance versus concentration. For alkyl hydrazones, $\varepsilon \sim 1800~{\rm M}^{-1}~{\rm cm}^{-1}$. For aryl hydrazones, $\varepsilon \sim 12000~{\rm M}^{-1}~{\rm cm}^{-1}$.

To determine reaction kinetic parameters, 50 μ M competitor was combined with 50 μ M BZA or HydAA (200 μ L total volume) and absorbance was repeatedly measured over a period of hours. After blank subtraction, the absorbance was converted to the concentration using the molar extinction coefficient. Using Matlab, the concentration over time was fit to a reversible biomolecular reaction rate 60 to determine the forward and reverse reaction rate:

$$x_{i}(t) = \frac{a_{+}(x_{0} - a_{-}) - a_{-}(x_{0} - a_{+})e^{-k_{1}(a_{+} - a_{-})t}}{(x_{0} - a_{-}) - (x_{0} - a_{+})e^{-k_{1}(a_{+} - a_{-})t}}$$
(3)

where

$$a_{+} = \frac{-k_{-1} + \sqrt{k_{-1}^2 + 4k_{1}k_{-1}x_{0}}}{2k_{1}} \tag{4}$$

$$a_{-} = \frac{-k_{-1} - \sqrt{k_{-1}^2 + 4k_1 k_{-1} x_0}}{2k_1} \tag{5}$$

To determine equilibrium concentration and half-time, we solved for infinite reaction time $(\lim_{t\to\infty}x(t)=a_+)$ and determined the time

required to reach $x(t_{1/2}) = \frac{1}{2}a_+$. To account for pipetting errors and differences in starting times, the initial concentration and time were unrestrained in the model fitting.

HELP and Competitor Rheology. All mechanical characterization of HELP formulations with or without competitors was performed by using a stress-controlled AR-G2 rheometer (TA Instruments). All tests were conducted on 50 μ L hydrogel samples, with 3–4 replicates per gel formulation. In this study, the competitor is mixed into the polymer precursor solutions first, and then, the solutions are mixed together to form a gel. During gelation, there is no surrounding bath. This means that the competitor has the opportunity to bind and impact gel formation without diffusing out of the gel.

All the competitors were prepared as 100 mM stock solutions in PBS. Competitors with an aldehyde group were premixed with HA solution, and competitors with a hydrazine group were premixed with ELP solution to achieve a final competitor concentration of 10 mM in HELP hydrogel. In some formulations (Figure 2B) 5% DMSO was added in the final gel formulation (e.g., 2.5 μ L in 50 μ L gel). All HELP formulations of 1 wt % HA-BZA and 2 wt % ELP-HYD were formed from stock solutions of 2 wt % HA and 4 wt % ELP dissolved in isotonic 10× PBS.

Rheology—Modulus. The modulus of HELP was characterized with small angle oscillatory shear (SAOS) with a 20 mm cone—plate geometry (1° cone angle, 28 μm gap between the geometry and stage). A 50 μL gel was formed from 25 μL of a 2 wt % HA solution pipetted onto the middle of the rheometer stage, followed by 25 μL of the 4 wt % ELP solution pipetted directly into the droplet of HA. The ELP was rapidly mixed into the HA using the pipet tip. The geometry head was immediately lowered onto the sample to close the geometry gap. To allow cross-links to fully form, the hydrogels were under 1% oscillatory strain and 1 rad/s angular frequency at 4 °C for 5 min, followed by a temperature ramp to 23 °C for 15 min, and finally a temperature ramp to 37 °C for 15 min. This protocol was immediately followed by a frequency sweep from 0.1 to 100 rad/s under 1% strain. The reported storage modulus (G') is taken from the linear region of the frequency sweep at 1 rad/s angular frequency.

Rheology—Gelation Time. To measure gelation time, $25~\mu L$ of 2 wt % HA and $25~\mu L$ of 4 wt % ELP were quickly mixed onto the middle of rheometer stage at 4 °C, and the geometry head was immediately lowered onto the sample to the geometry gap. A timer was started as soon as the polymer solutions came into contact with

each other and the gelation time was defined following the Winters–Chambon criteria, i.e., the time required to reach the for the storage modulus (G') to be greater than the loss modulus (G'').

Rheology—Recovery. HELP hydrogels (50 μ L, 1 wt % HA and 2 wt % ELP) with or without competitors were made on ice in 7 mm diameter molds. To allow for cross-links to fully form, hydrogels were incubated on ice for 10 min, followed by 15 min at room temperature and 15 min at 37 °C. Then 1 mL of PBS was added to each well and all the samples were incubated at 37 °C before measurement. Media changes were performed every 24 h.

Mechanical recovery was characterized using SAOS with an 8 mm cone—plate geometry. Hydrogels were carefully removed from the molds and placed in the rheometer stage. The geometry head was lowered onto the sample to a gap size of $1000~\mu\text{m}$, and hydrogel samples were characterized under a frequency sweep from 0.1 to 100~rad/s at 1% strain at $37~^\circ\text{C}$. The reported storage modulus (G') is taken from the linear region of the frequency sweep at 1~rad/s angular frequency. Characterization was performed on 3-4~replicates per gel condition, and data was normalized by the storage modulus of a control HELP formulation without competitors on each day.

Fluorescence Recovery after Photobleaching—Diffusion Rates in HELP. HELP (50 μ L) was prepared within a well of a clear-bottom half area, black 96-well plate (Greiner Bio-One 675090). During hydrogel gelation, 4 mg/mL fluorescein isothiocyanate (FITC)-labeled dextran (Sigma) of varying molecular weights (20, 40, 70, 150 kDa) was mixed and allowed to gel for 30 min as above. Fluorescent images were taken using a confocal microscope (Leica SPE) where a 100 μ m × 100 μ m area in each matrix was photobleached using a 488 nm laser at 100% intensity for 30 s. FITC-dextran recovery into the photobleached region was monitored for over 90 s. Images were analyzed using a previously published technique with an accompanying open-source Matlab code "frap_analysis". The diffusivity of small molecules was extrapolated from a linear fit of the Rouse regime (Figure S8). 79 N = 4 hydrogels were analyzed for each FITC-dextran molecular weight.

Limits of Sol–Gel Formation—Phase Diagram. To assemble a phase diagram that delineates combinations of equilibrium constants and competitor concentrations that permit formation of a gel, we took advantage of the dependence of the (1) competitor reaction and (2) cross-linking reaction on the concentration of A (Figure 2A). Using this relationship, the equilibrium concentrations of each component in the system were related to the ratio of the equilibrium constants ($K_{\rm eq,1}$ and $K_{\rm eq,2}$). The extent of the cross-linking reaction was related to the ability to form a hydrogel using percolation theory. The combinations of reaction stability ($K_{\rm eq}$) and concentrations of competitor that allow formation of a gel were determined by the critical extent of reaction. Percolation theory was used to calculate the critical extent of reaction (p_c) from the average functionality of HA and ELP, 102.8 and 12.6, respectively. A more detailed description of this approach can be found in Methods S1.

Gelation Time Model. The Matlab ode45 function was used to numerically solve the system of coupled reaction rate equations that describe the competing competitor and cross-linking reactions:

$$\frac{\partial [\mathbf{A}]}{\partial t} = -k_1[\mathbf{A}][\mathbf{C}] + k_{-1}[\mathbf{A}\mathbf{C}] - k_2[\mathbf{A}][\mathbf{B}] + k_{-2}[\mathbf{A}\mathbf{B}]$$
 (6)

$$\frac{\partial[\mathbf{C}]}{\partial t} = -k_1[\mathbf{A}][\mathbf{C}] + k_{-1}[\mathbf{A}\mathbf{C}] \tag{7}$$

$$\frac{\partial [AC]}{\partial t} = k_1[A][C] - k_{-1}[AC]$$
(8)

$$\frac{\partial[\mathbf{B}]}{\partial t} = -k_2[\mathbf{A}][\mathbf{B}] + k_{-2}[\mathbf{A}\mathbf{B}] \tag{9}$$

$$\frac{\partial[AB]}{\partial t} = k_2[A][B] - k_{-1}[AB] \tag{10}$$

The gelation time was defined as the time required to reach a sufficient concentration of cross-links (AB) such that a percolated

network is formed. Using Matlab, the extent of the cross-linking reaction was calculated as $\frac{[B]_0-[B]}{[B]_0}$, where $[B]_0$ is the initial concentration of B and [B] is the instantaneous concentration. The critical extent of cross-linking reaction (p_c) required to form a gel was calculated from the averaged functionality (f) of HA and ELP following percolation theory: $p_c=\frac{1}{f-1}$. The gelation time was set as the time required for the extent of the cross-linking reaction $\left(\frac{[B]_0-[B]}{[B]_0}\right)$

) to reach p_c . This process was repeated over a large range of concentrations of competitor. The initial concentration for each species was: $[A]_0 = [B]_0 = 7.4$ mM, $[AC]_0 = [AB]_0 = 0$ mM, $[C]_0 = 10$ mM. The gelation time was normalized to a control HELP formulation with no competitor ($[C]_0 = 0$ mM).

HELP Fluorescent Imaging. HELP gels (1 wt % HA and 2 wt % ELP) were made in 4 mm molds following the procedure outlined above. Rhodamine B dye (2 mg/mL; Sigma 81-88-9) and either 0 or 10 mM Butanal were added to the HA precursor solution prior to mixing with ELP precursor solution and HELP formation. Fluorescent images of HELP with and without competitor (0 and 10 mM Butanal; 1 mg/mL Rhodamine B) were taken using a confocal microscope (Leica SPE) under a 10× objective using a 488 nm laser. Pixel intensity of each image was analyzed with ImageJ (NIH, v.2.1.0/1.53c). Five gels were made in each condition, and three images were taken from each gel.

Experimental Release Profile. HELP gels (1 wt % HA and 2 wt % ELP) were made in 4 mm molds following the procedure above. Rhodamine aldehyde (5.6 mM; AAT Bioquest 9005) was added to the HA precursor solution prior to mixing (2.8 mM final concentration). Following gelation, hydrogels were submerged in 1 mL of PBS at 37 °C in a humidified incubator. At each time point, 30 μ L of the solution was removed to quantify the total fluorescence (556/580 nm) of rhodamine aldehyde released into the bath. The total fluorescence was normalized by a control 2.8 mM rhodamine aldehyde solution. PBS medium changes were performed daily.

Diffusion Model. The Matlab pdepe function was used to numerically solve the system of coupled reaction-diffusion equations that describe both the competitor and cross-linking reactions and the diffusion of the competitor into the surrounding sink. Using the symmetry of the hydrogel, the model was simplified to one spatial dimension, x, corresponding to the height of the gel.

$$\frac{\partial[A]}{\partial t} = -k_1[A][C] + k_{-1}[AC] - k_2[A][B] + k_{-2}[AB]$$
 (11)

$$\frac{\partial [C]}{\partial t} = D \frac{\partial^2 C}{\partial x^2} - k_1 [A][C] + k_{-1} [AC]$$
(12)

$$\frac{\partial[AC]}{\partial t} = k_1[A][C] - k_{-1}[AC]$$
(13)

$$\frac{\partial[\mathbf{B}]}{\partial t} = -k_2[\mathbf{A}][\mathbf{B}] + k_{-2}[\mathbf{A}\mathbf{B}] \tag{14}$$

$$\frac{\partial[AB]}{\partial t} = k_2[A][B] - k_{-1}[AB] \tag{15}$$

To numerically solve this system, the initial conditions and boundary conditions were specified depending on the experiment being modeled (Methods S1). For each model (rhodamine aldehyde release and modulus recovery), the boundary condition at the bottom of the hydrogel (x=0) was a Neumann condition of zero flux to match the impermeable bottom of the culture plate. At the interface of the hydrogel and sink (x=L), the boundary condition for all immobile species (cross-linking sites) was also set to a Neumann condition of zero flux. To model the release rate, the boundary condition of rhodamine aldehyde at the top of the gel was set to an infinite sink, e.g., a Dirichlet condition of [C]=0 mM. To model the modulus recovery, the boundary condition of the competitor was initially set to a Dirichlet condition of [C]=0 mM and the system was solved over a short time period of τ . The total concentration of competitor released

into the surrounding sink after a period of τ was then set as the new boundary condition, $[C](x=L,t=\tau_1)=\frac{1}{20}[C]_1$, assuming a 20-fold dilution (50 μ L gel into 1 mL bath). This was repeated over the entire time period of the model, with a minimum of 50 steps (τ_n , where n > 50). To model media changes, the boundary condition was reset to [C] = 0 mM at appropriate time points, e.g., every 24 h.

Initial conditions were calculated using the Matlab ode45 function, assuming a closed system with no diffusion of competitor, as in Methods S2. Reaction rate parameters were empirically determined (Table 1) and the diffusion coefficient calculated from extrapolation of the diffusion of FITC-dextran probes (Figure S8). For cross-linking recovery (Figure 4B,C) the cross-linking concentration ([AB]) was normalized to the predicted equilibrium cross-linking concentration with no competitor present.

Cell Culture and Encapsulation. Intestinal Organoid Encapsulation. To form cell-laden HELP hydrogels (1 wt % HA and 2 wt % ELP), 2× stock solutions of 2 wt % HA and 4 wt % ELP were dissolved in 10× PBS. For HELP formulations with competitor, 20 mM Butanal was added to the 2× HA solution. To vary the concentration of the fibronectin binding domain RGDS, ELP with the RGDS motif was combined with ELP with the scrambled binding domain RDGS to maintain a constant ELP content. Human intestinal organoids were cultured in maintenance media in a commercially available Engelbreth-Holm-Swarm matrix (Cultrex) and dissociated into single cell suspensions prior to HELP encapsulation following previously reported protocols.⁴⁹ The desired number of cells were centrifuged for 5 min at 500g and resuspended in a 2× stock solution of ELP. To form 10 μL cell-laden HELP gels (1 wt % HA and 2 wt % ELP; 7.5×10^5 to 1.0×10^6 cells/mL), 5 μ L of HA solution was first added to a custom 4 mm diameter silicone mold affixed to a glass coverslip within a 24 well plate. Then an equal volume of 2× stock ELP-cell solution was pipetted directly onto the HA and immediately mixed using the same pipet tip. The hydrogels were incubated at 4 °C for 10 min, followed by another 10 min at RT and a final incubation at 37 °C for 10 min to ensure complete gelation. Following gelation, HELP hydrogels were submerged in intestinal organoid growth media (outlined below), with media changes every 3 days.

Intestinal organoid growth media consisted of a 1:1 mixture of ADMEM-F12 media (Thermo Fisher Scientific, Waltham, MA) and L-WRN (ATCC CRL3276) conditioned media. L-WRN conditioned media was produced as previously reported from transgenic cells encoded for Wnt-3A, R-spondin 3, and Noggin production. 49 The 1:1 mixture was supplemented with the following reagents: 1 mM HEPES (4-(2-hydroxyethyl)-1-piperazineethanesulfonic acid, Thermo Fisher Scientific, Waltham, MA), 1× Glutamax (Thermo Fisher Scientific, Waltham, MA), 10 mM nicotinamide (Sigma-Aldrich, St. Louis, MO), 1 mM N-acetylcysteine (Sigma-Aldrich, St. Louis, MO), 1× B-27 supplement (Thermo Fisher Scientific, Waltham, MA), 0.5 μ M A83-01 (Sigma-Aldrich, St. Louis, MO), 1× PSQ (Thermo Fisher Scientific, Waltham, MA), 10 nM Gastrin-I (Sigma-Aldrich, St. Louis, MO), 10 μM SB-202190 (Bio-Techne, Minneapolis, MN), 50 ng/mL recombinant EGF (Thermo Fisher Scientific, Waltham, MA), and 1× Normocin (InvivoGen, San Diego, CA). Small molecule inhibitors, 10 μM Y-27632, and 2.5 μM CHIR-99021 (Bio-Techne, Minneapolis, MN) were added to the medium for the first 3 days only.

Growth Rate and Efficiency Study. To analyze organoid formation efficiency, bright-field images of each well were taken at 20× magnification on day 3 via phase contrast (Leica Microsystems, THUNDER Imager 3D Cell Culture). For each gel, at least 3 nonoverlapping fields of view were chosen, and a ~100 μ m z-stack with 10 z-slices was taken in every field of view. Using the size of each image, organoid formation efficiency for each gel was calculated by the organoid count per volume (~100 μ m) and compared to the initial cell seeding density. At least 3 fields of view from three replicate hydrogels were used for each HELP formulation. To measure organoid growth rate, gels were imaged every 3 days (days 0 to 9) using a 10× objective. At least 9 nonoverlapping images were taken of N=3 replicate hydrogels for each HELP formulation. Organoid

diameter was measured by manually drawing a circle over each organoid using ImageJ (NIH, v.2.1.0/1.53c).

Immunocytochemistry. To prepare samples for fixation, each HELP hydrogel was washed briefly with prewarmed PBS. Cells were fixed by adding 750 µL of prewarmed 4% paraformaldehyde (PFA) for 20 min. The fixation solution was then removed, and three 10 min washes of PBS were performed. Cells were permeabilized for 1 h with 0.5% v/v Triton X-100 in PBS (PBST) and then blocked for 3 h in PBS with 5% v/v goat serum and 0.1% v/v Triton X-100. Primary antibodies (ZO-1, Thermo Fisher 33-9100; β -catenin, Cell Signaling 8480) were diluted (1:150) in PBS with 2.5 wt % BSA, 2.5% v/v goat serum, and 0.5% v/v Triton X-100 (Antibody Dilution Solution), and samples were stained overnight at 4 °C. Antibody solutions were removed, and three 20 min washes in PBST were performed. Secondary antibodies were diluted 1:500 in Antibody Dilution Solution and incubated overnight at 4 °C. The secondary antibody solution was then removed, and the samples were washed three times with PBST for 20 min. Samples were stained with DAPI (5 mg/mL stock, 1:2000) and tetramethylrhodamine (TRITC)-phalloidin (100 μg/mL in DMSO stock, 1:400) in 0.1% v/v Triton X-100 in PBS (PBST) for 2 h at RT. Samples then were washed with PBST (3×10 min) and imaged using a confocal microscope (Leica SPE).

Lactate Dehydrogenase—Metric of Cytotoxicity. Lactate dehydrogenase was measured using LDH-GloTM Cytotoxicity Assay (Promega) to quantify competitor cytotoxicity. Intestinal organoids were cultured in HELP formulations, as outlined above. Every 3 days, from day 0 to day 9, $10~\mu$ L of culture media was taken from each well and stored in LDH storage buffer (200 mM Tris-HCl (pH 7.3), 10% Glycerol, 1% BSA) at -80 °C until measurement. Following the assay instructions, the relative LDH concentration was measured via luminescence. To normalize to the maximum possible cytotoxicity, on day 9 the cells were permeabilized with 0.2~w/v Triton X-100 for 2 h as a positive control. Percentage cytotoxicity was normalized to the control at each condition and then normalized to the HELP formulation with no competitor (0 mM Butanal) at each time point. N=4 replicates for each condition were analyzed.

ASSOCIATED CONTENT

Supporting Information

The Supporting Information is available free of charge at https://pubs.acs.org/doi/10.1021/acs.chemmater.3c01575.

Additional experimental details and methods, including ¹H NMR spectra for all compounds, kinetic models, development of gelation and diffusion models, and code of the release model (PDF)

AUTHOR INFORMATION

Corresponding Author

Sarah C. Heilshorn — Department of Materials Science & Engineering, Stanford University, Stanford, California 94305, United States; oocid.org/0000-0002-9801-6304; Email: heilshorn@stanford.edu

Authors

Aidan E. Gilchrist – Department of Materials Science & Engineering, Stanford University, Stanford, California 94305, United States; orcid.org/0000-0003-3536-1044

Yueming Liu — Department of Materials Science & Engineering, Stanford University, Stanford, California 94305, United States

Katarina Klett – Stem Cell Biology and Regenerative Medicine, Stanford University, Stanford, California 94305, United States

Yu-Chung Liu — Department of Materials Science and Engineering, National Tsing Hua University, Hsinchu City 300, Taiwan Sofia Ceva – Department of Materials Science & Engineering, Stanford University, Stanford, California 94305, United States

Complete contact information is available at: https://pubs.acs.org/10.1021/acs.chemmater.3c01575

Author Contributions

*A.E.G. and Y.L. contributed equally to this work. A.E.G. and Y.L. performed conceptualization, investigation, data curation, validation, formal analysis, methodology, visualization, and writing - original draft and review and editing. K.K. performed methodology, investigation, validation, and writing - review and editing. Y.-C.L. and S.C. performed formal analysis, methodology, and writing - review and editing. S.C.H. performed conceptualization, supervision, funding acquisition, writing - original draft and review and editing.

Note

Any opinions, findings, and conclusions or recommendations expressed in this material are those of the author(s) and do not necessarily reflect the views of the National Science Foundation.

The authors declare the following competing financial interest(s): SCH, YL, and AEG are named inventors on a provisional patent application submitted by Stanford University describing part of this work.

ACKNOWLEDGMENTS

Research reported in this publication was supported by the National Science Foundation (CBET 2033302 to S.C.H.) and the National Institutes of Health (R01 EB027171, R01 HL142718, and R01 HL151997 to S.C.H.).

■ REFERENCES

- (1) Lee, K. Y.; Mooney, D. J. Hydrogels for tissue engineering. *Chem. Rev.* **2001**, *101*, 1869–1879.
- (2) Peppas, N. A.; Hilt, J. Z.; Khademhosseini, A.; Langer, R. Hydrogels in biology and medicine: From molecular principles to bionanotechnology. *Adv. Mater.* **2006**, *18*, 1345–1360.
- (3) Wang, H.; Cai, L.; Paul, A.; Enejder, A.; Heilshorn, S. C. Hybrid elastin-like polypeptide-polyethylene glycol (ELP-PEG) hydrogels with improved transparency and independent control of matrix mechanics and cell ligand density. *Biomacromolecules* **2014**, *15*, 3421–3428
- (4) Drury, J. L.; Mooney, D. J. Hydrogels for tissue engineering: scaffold design variables and applications. *Biomaterials* **2003**, *24*, 4337–4351.
- (5) Burdick, J. A.; Stevens, M. M. In *Biomaterials, Artificial Organs and Tissue Engineering*; Woodhead Publishing: 2005; pp 107–115.
- (6) Ho, S. S.; Keown, A. T.; Addison, B.; Leach, J. K. Cell Migration and Bone Formation from Mesenchymal Stem Cell Spheroids in Alginate Hydrogels Are Regulated by Adhesive Ligand Density. *Biomacromolecules* **2017**, *18*, 4331–4340.
- (7) Saraswathibhatla, A.; Indana, D.; Chaudhuri, O. Cellextracellular matrix mechanotransduction in 3D. *Nat. Rev. Mol. Cell Biol.* **2023**, *24*, 495–516.
- (8) Rizwan, M.; Baker, A. E. G.; Shoichet, M. S. Designing Hydrogels for 3D Cell Culture Using Dynamic Covalent Crosslinking. *Adv. Healthc Mater.* **2021**, *10*, No. e2100234.
- (9) Wang, H.; Heilshorn, S. C. Adaptable Hydrogel Networks with Reversible Linkages for Tissue Engineering. *Adv. Mater.* **2015**, 27, 3717–3736
- (10) Gilchrist, A. E.; Harley, B. A. C. Engineered Tissue Models to Replicate Dynamic Interactions within the Hematopoietic Stem Cell Niche. *Adv. Healthc Mater.* **2022**, *11*, No. e2102130.

- (11) Lou, J.; Stowers, R.; Nam, S.; Xia, Y.; Chaudhuri, O. Stress relaxing hyaluronic acid-collagen hydrogels promote cell spreading, fiber remodeling, and focal adhesion formation in 3D cell culture. *Biomaterials* **2018**, *154*, 213–222.
- (12) Chaudhuri, O.; et al. Hydrogels with tunable stress relaxation regulate stem cell fate and activity. *Nat. Mater.* **2016**, *15*, 326–334.
- (13) Chaudhuri, O.; et al. Substrate stress relaxation regulates cell spreading. *Nat. Commun.* **2015**, *6*, 6364.
- (14) Gilchrist, A. E.; Lee, S.; Hu, Y.; Harley, B. A. C. Soluble Signals and Remodeling in a Synthetic Gelatin-Based Hematopoietic Stem Cell Niche. *Adv. Healthc Mater.* **2019**, *8*, No. e1900751.
- (15) Muir, V. G.; Burdick, J. A. Chemically Modified Biopolymers for the Formation of Biomedical Hydrogels. *Chem. Rev.* **2021**, *121*, 10908–10949.
- (16) Raeber, G. P.; Lutolf, M. P.; Hubbell, J. A. Molecularly engineered PEG hydrogels: a novel model system for proteolytically mediated cell migration. *Biophys. J.* **2005**, *89*, 1374–1388.
- (17) Stevens, K. R.; Miller, J. S.; Blakely, B. L.; Chen, C. S.; Bhatia, S. N. Degradable hydrogels derived from PEG-diacrylamide for hepatic tissue engineering. *J. Biomed Mater. Res. A* **2015**, *103*, 3331–3338.
- (18) Mantooth, S. M.; Munoz-Robles, B. G.; Webber, M. J. Dynamic Hydrogels from Host-Guest Supramolecular Interactions. *Macromol. Biosci* **2019**, *19*, No. e1800281.
- (19) Hu, W.; Wang, Z.; Xiao, Y.; Zhang, S.; Wang, J. Advances in crosslinking strategies of biomedical hydrogels. *Biomater Sci.* **2019**, *7*, 843–855.
- (20) Steele, A. N.; et al. A Biocompatible Therapeutic Catheter-Deliverable Hydrogel for In Situ Tissue Engineering. *Adv. Healthcare Mater.* **2019**, *8*, 1801147.
- (21) Wong Po Foo, C. T.; Lee, J. S.; Mulyasasmita, W.; Parisi-Amon, A.; Heilshorn, S. C. Two-component protein-engineered physical hydrogels for cell encapsulation. *Proc. Natl. Acad. Sci. U. S. A.* **2009**, 106, 22067–22072.
- (22) Madl, C. M.; Heilshorn, S. C. Rapid Diels—Alder Cross-linking of Cell Encapsulating Hydrogels. *Chem. Mater.* **2019**, *31*, 8035–8043.
- (23) McKinnon, D. D.; Domaille, D. W.; Cha, J. N.; Anseth, K. S. Biophysically Defined and Cytocompatible Covalently Adaptable Networks as Viscoelastic 3D Cell Culture Systems. *Adv. Mater.* **2014**, 26, 865–872.
- (24) Tang, S. C.; Richardson, B. M.; Anseth, K. S. Dynamic covalent hydrogels as biomaterials to mimic the viscoelasticity of soft tissues. *Prog. Mater. Sci.* **2021**, *120*, 100738.
- (25) Rosales, A. M.; Anseth, K. S. The design of reversible hydrogels to capture extracellular matrix dynamics. *Nat. Rev. Mater.* **2016**, *1*, 15012.
- (26) FitzSimons, T. M.; Oentoro, F.; Shanbhag, T. V.; Anslyn, E. V.; Rosales, A. M. Preferential Control of Forward Reaction Kinetics in Hydrogels Crosslinked with Reversible Conjugate Additions. *Macromolecules* **2020**, *53*, 3738–3746.
- (27) Morgan, F. L. C.; Fernandez-Perez, J.; Moroni, L.; Baker, M. B. Tuning Hydrogels by Mixing Dynamic Cross-Linkers: Enabling Cell-Instructive Hydrogels and Advanced Bioinks. *Adv. Healthc Mater.* **2022**, *11*, No. e2101576.
- (28) Hui, E.; Sumey, J. L.; Caliari, S. R. Click-functionalized hydrogel design for mechanobiology investigations. *Mol. Syst. Des Eng.* **2021**, *6*, 670–707.
- (29) Kool, E. T.; Park, D. H.; Crisalli, P. Fast hydrazone reactants: electronic and acid/base effects strongly influence rate at biological pH. J. Am. Chem. Soc. 2013, 135, 17663–17666.
- (30) Saito, F.; Noda, H.; Bode, J. W. Critical evaluation and rate constants of chemoselective ligation reactions for stoichiometric conjugations in water. *ACS Chem. Biol.* **2015**, *10*, 1026–1033.
- (31) Rowan, S. J.; Cantrill, S. J.; Cousins, G. R.; Sanders, J. K.; Stoddart, J. F. Dynamic covalent chemistry. *Angew. Chem., Int. Ed. Engl.* **2002**. *41*, 898–952.
- (32) Gilchrist, A. E.; et al. Encapsulation of murine hematopoietic stem and progenitor cells in a thiol-crosslinked maleimide-functionalized gelatin hydrogel. *Acta Biomater* **2021**, *131*, 138–148.

- (33) Jansen, L. E.; Negron-Pineiro, L. J.; Galarza, S.; Peyton, S. R. Control of thiol-maleimide reaction kinetics in PEG hydrogel networks. *Acta Biomater* **2018**, *70*, 120–128.
- (34) Darling, N. J.; Hung, Y. S.; Sharma, S.; Segura, T. Controlling the kinetics of thiol-maleimide Michael-type addition gelation kinetics for the generation of homogenous poly(ethylene glycol) hydrogels. *Biomaterials* **2016**, *101*, 199–206.
- (35) Wang, H.; et al. Transient supramolecular hydrogels formed by catalytic control over molecular self-assembly. *Soft Matter* **2020**, *16*, 9406–9409.
- (36) Karvinen, J.; et al. Soft hydrazone crosslinked hyaluronan- and alginate-based hydrogels as 3D supportive matrices for human pluripotent stem cell-derived neuronal cells. *React. Funct. Polym.* **2018**, *124*, 29–39.
- (37) Patenaude, M.; Campbell, S.; Kinio, D.; Hoare, T. Tuning gelation time and morphology of injectable hydrogels using ketone-hydrazide cross-linking. *Biomacromolecules* **2014**, *15*, 781–790.
- (38) Mueller, E.; Xu, F.; Hoare, T. FRESH Bioprinting of Dynamic Hydrazone-Cross-Linked Synthetic Hydrogels. *Biomacromolecules* **2022**, 23, 4883–4895.
- (39) Wang, L. L.; et al. Three-dimensional extrusion bioprinting of single- and double-network hydrogels containing dynamic covalent crosslinks. *J. Biomed Mater. Res. A* **2018**, *106*, 865–875.
- (40) Kalia, J.; Raines, R. T. Hydrolytic Stability of Hydrazones and Oximes. *Angew. Chem., Int. Ed.* **2008**, 47, 7523–7526.
- (41) Wang, H.; et al. Covalently adaptable elastin-like protein hyaluronic acid (ELP HA) hybrid hydrogels with secondary thermoresponsive crosslinking for injectable stem cell delivery. *Adv. Funct Mater.* **2017**, 27, 1605609.
- (42) Navarro, R. S.; et al. Tuning Polymer Hydrophilicity to Regulate Gel Mechanics and Encapsulated Cell Morphology. *Adv. Healthc Mater.* **2022**, *11*, No. e2200011.
- (43) Madl, C. M.; Katz, L. M.; Heilshorn, S. C. Bio-Orthogonally Crosslinked, Engineered Protein Hydrogels with Tunable Mechanics and Biochemistry for Cell Encapsulation. *Adv. Funct Mater.* **2016**, *26*, 3612–3620.
- (44) LeSavage, B. L.; Suhar, N. A.; Madl, C. M.; Heilshorn, S. C. Production of Elastin-like Protein Hydrogels for Encapsulation and Immunostaining of Cells in 3D. *J. Vis Exp* **2018**, 57739.
- (45) Burdick, J. A.; Prestwich, G. D. Hyaluronic Acid Hydrogels for Biomedical Applications. *Adv. Mater.* **2011**, 23, H41–H56.
- (46) Dicker, K. T.; et al. Hyaluronan: a simple polysaccharide with diverse biological functions. *Acta Biomater* **2014**, *10*, 1558–1570.
- (47) Zhu, D.; Wang, H.; Trinh, P.; Heilshorn, S. C.; Yang, F. Elastin-like protein-hyaluronic acid (ELP-HA) hydrogels with decoupled mechanical and biochemical cues for cartilage regeneration. *Biomaterials* **2017**, *127*, 132–140.
- (48) Suhar, R. A.; et al. Hyaluronan and elastin-like protein (HELP) gels significantly improve microsphere retention in the myocardium. *Biomater Sci.* **2022**, *10*, 2590–2608.
- (49) Hunt, D. R.; et al. Engineered Matrices Enable the Culture of Human Patient-Derived Intestinal Organoids. *Adv. Sci.* (Weinh) 2021, 8. 2004705.
- (50) LeSavage, B. L. Engineered extracellular matrices reveal stiffness-mediated chemoresistance in patient-derived pancreatic cancer organoids. *BioRxiv*, 2022.2004.2022.488943, 2022, DOI: 10.1101/2022.04.22.488943.
- (51) Hull, S. M.; et al. 3D bioprinting of dynamic hydrogel bioinks enabled by small molecule modulators. *Sci. Adv.* **2023**, *9*, No. eade7880.
- (52) Lou, J.; Xia, Y. Using Competitor Molecules to Reversibly Modulate the Mechanical Properties of Viscoelastic Hydrogels. *ACS Macro Lett.* **2022**, *11*, 1312–1316.
- (53) Teng, L.; Chen, Y.; Jia, Y. G.; Ren, L. Supramolecular and dynamic covalent hydrogel scaffolds: from gelation chemistry to enhanced cell retention and cartilage regeneration. *J. Mater. Chem. B* **2019**, *7*, 6705–6736.

- (54) Kolmel, D. K.; Kool, E. T. Oximes and Hydrazones in Bioconjugation: Mechanism and Catalysis. *Chem. Rev.* **2017**, *117*, 10358–10376.
- (55) Jencks, W. P. Mechanism and Catalysis of Simple Carbonyl Group Reactions. *Prog. Phys. Org. Chem.* **1964**, *2*, 63–128.
- (56) Shayan, M.; et al. Elastin-like protein hydrogels with controllable stress relaxation rate and stiffness modulate endothelial cell function. *J. Biomed Mater. Res. A* **2023**, *111*, 896–909.
- (57) Winne, J. M.; Leibler, L.; Du Prez, F. E. Dynamic covalent chemistry in polymer networks: a mechanistic perspective. *Polym. Chem.* **2019**, *10*, 6091–6108.
- (58) McKinnon, D. D.; Domaille, D. W.; Cha, J. N.; Anseth, K. S. Biophysically defined and cytocompatible covalently adaptable networks as viscoelastic 3D cell culture systems. *Adv. Mater.* **2014**, 26, 865–872.
- (59) Mayerhofer, T. G.; Pahlow, S.; Popp, J. The Bouguer-Beer-Lambert Law: Shining Light on the Obscure. *ChemPhysChem* **2020**, 21, 2029–2046.
- (60) Dirksen, A.; Dirksen, S.; Hackeng, T. M.; Dawson, P. E. Nucleophilic catalysis of hydrazone formation and transimination: implications for dynamic covalent chemistry. *J. Am. Chem. Soc.* **2006**, 128, 15602–15603.
- (61) Rubinstein, M.; Colby, R. H. Random branching and gelation. In *Polymer Physics*; Oxford University Press: 2003; pp 199–252.
- (62) De Gennes, P. G. On a relation between percolation theory and the elasticity of gels. *J. Phys., Lett.* **1976**, *37*, 1–2.
- (63) Stockmayer, W. H. Theory of Molecular Size Distribution and Gel Formation in Branched-Chain Polymers. *J. Chem. Phys.* **1943**, *11*, 45–55.
- (64) Flory, P. J. Molecular Size Distribution in Three Dimensional Polymers. I. Gelation 1. J. Am. Chem. Soc. 1941, 63, 3083–3090.
- (65) Gjorevski, N.; et al. Designer matrices for intestinal stem cell and organoid culture. *Nature* **2016**, *539*, 560–564.
- (66) Gjorevski, N.; et al. Tissue geometry drives deterministic organoid patterning. *Science* **2022**, *375*, No. eaaw9021.
- (67) Hernandez-Gordillo, V.; et al. Fully synthetic matrices for in vitro culture of primary human intestinal enteroids and endometrial organoids. *Biomaterials* **2020**, *254*, 120125.
- (68) Cruz-Acuna, R.; et al. PEG-4MAL hydrogels for human organoid generation, culture, and in vivo delivery. *Nat. Protoc* **2018**, 13, 2102–2119.
- (69) Cruz-Acuna, R.; et al. Synthetic hydrogels for human intestinal organoid generation and colonic wound repair. *Nat. Cell Biol.* **2017**, 19, 1326–1335.
- (70) Rezakhani, S.; Gjorevski, N.; Lutolf, M. P. Low-Defect Thiol-Michael Addition Hydrogels as Matrigel Substitutes for Epithelial Organoid Derivation. *Adv. Funct. Mater.* **2020**, *30*, 2000761.
- (71) Co, J. Y.; Margalef-Catala, M.; Monack, D. M.; Amieva, M. R. Controlling the polarity of human gastrointestinal organoids to investigate epithelial biology and infectious diseases. *Nat. Protoc* **2021**, *16*, 5171–5192.
- (72) Zou, W. Y.; et al. Human Intestinal Enteroids: New Models to Study Gastrointestinal Virus Infections. *Methods Mol. Biol.* **2017**, 1576, 229–247.
- (73) Sato, T.; Clevers, H. Growing self-organizing mini-guts from a single intestinal stem cell: mechanism and applications. *Science* **2013**, 340, 1190–1194.
- (74) Sato, T.; et al. Long-term expansion of epithelial organoids from human colon, adenoma, adenocarcinoma, and Barrett's epithelium. *Gastroenterology* **2011**, *141*, 1762–1772.
- (75) Fritz, K. S.; Petersen, D. R. An overview of the chemistry and biology of reactive aldehydes. *Free Radic Biol. Med.* **2013**, *59*, 85–91.
- (76) Swinehart, D. F. The Beer-Lambert Law. J. Chem. Educ. 1962, 39, 333.
- (77) Winter, H. H.; Chambon, F. Analysis of Linear Viscoelasticity of a Crosslinking Polymer at the Gel Point. *J. Rheol.* **1986**, *30*, 367–382.

- (78) Jonsson, P.; Jonsson, M. P.; Tegenfeldt, J. O.; Hook, F. A method improving the accuracy of fluorescence recovery after photobleaching analysis. *Biophys. J.* **2008**, *95*, 5334–5348.
- (79) Pluen, A.; Netti, P. A.; Jain, R. K.; Berk, D. A. Diffusion of macromolecules in agarose gels: comparison of linear and globular configurations. *Biophys. J.* **1999**, *77*, 542–552.